1   **Sulfur isotopes in rivers: Insights into global weathering budgets, pyrite**

2   **oxidation, and the modern sulfur cycle**

3

4

5   Andrea Burke[1,2], Theodore M. Present[2] , Guillaume Paris[2,3], Emily C. M. Rae[1],

6   Brodie H. Sandilands[1], Jérôme Gaillardet[4], Bernhard Peucker-Ehrenbrink[5],

7   Woodward W. Fischer[2], James W. McClelland[6], Robert G.M. Spencer[7], Britta M.

8   Voss[5], Jess F. Adkins[2]

9

10   [1] University of St Andrews, St Andrews, UK;

11   [2]California Institute of Technology, Pasadena, CA, USA

12   [3]CRPG – CNRS, Vandoeuvre-lès-Nancy, France

13   [4]Institut de Physique du Globe de Paris, Paris, France

14   [5]Woods Hole Oceanographic Institution, Woods Hole, MA, USA

15   [6]University of Texas at Austin, Austin, TX, USA

16   [7]Florida State University, Tallahassee, FL, USA

17

18

19

20

22

23

24

25

26   **Abstract**

27   The biogeochemical sulfur cycle is intimately linked to the cycles of

28   carbon, iron, and oxygen, and plays an important role in global climate via

29   weathering reactions and aerosols. However, many aspects of the modern

30   budget of the global sulfur cycle are not fully understood. We present new $\delta^{34}S$

31   measurements on sulfate from more than 160 river samples from different

32   geographical and climatic regions—more than 46% of the world's freshwater

33   flux to the ocean is accounted for in this estimate of the global riverine sulfur

34   isotope budget. These measurements include major rivers and their tributaries,

35   as well as time series, and are combined with previously published data to

36   estimate the modern flux-weighted global riverine $\delta^{34}S$ as 4.4 ± 4.5 ‰ (V-CDT),

37   and 4.8 ± 4.9 ‰ when the most polluted rivers are excluded. Combined with

38   major anion and cation concentrations, the sulfur isotope data allow us to tease

39   apart the relative contributions of different processes to the modern riverine

40   sulfur budget, resulting in new estimates of the flux of riverine sulfate due to the

41   oxidative weathering of pyrites (1.3 ± 0.2 Tmol S/y) and the weathering of

42   sedimentary sulfate minerals (1.5 ± 0.2 Tmol S/y). These data indicate that

43   previous estimates of the global oxidative weathering of pyrite have been too

44   low by a factor of two. As pyrite oxidation coupled to carbonate weathering can

45   act as a source of CO_2 to the atmosphere, this global pyrite weathering budget

46   implies that the global CO_2 weathering sink is overestimated. Furthermore, the

47   large range of sulfur isotope ratios in modern rivers indicates that secular

48   changes in the lithologies exposed to weathering through time could play a major

49   role in driving past variations in $\delta^{34}S$ of seawater.

50

51

1 Introduction

The biogeochemical sulfur cycle is intimately linked to the cycles of

carbon and oxygen (e.g. Berner and Raiswell, 1983). Reconstructing the sources

and sinks of sulfur to the marine environment in the past is thus important for

understanding long-term changes in climate and the redox processes operating

in Earth's surface environments. The sulfur isotope compositions of sources and

sinks provide a sensitive tracer of the processes that drive the sulfur cycle

because there are large isotope fractionations that occur associated with cycling

sulfur between oxidized and reduced phases (e.g. Garrels and Lerman, 1984).

Microbial sulfate reduction, for instance, imparts a large S isotope fractionation

($\varepsilon \approx 0$ to -70‰ (e.g. Habicht and Canfield, 2001; Sim et al., 2011)), leaving—on

average—pyrite and other sulfide-bearing minerals with lower sulfur isotope

ratios than seawater and sedimentary sulfate.

Reconstructions of sulfur isotope ratios through geologic time from

marine sedimentary rocks have typically been used to infer past changes in the

burial flux of reduced sulfur (pyrite) relative to the removal of oxidized sulfur in

the form of sulfate (evaporite deposits) (Kump and Garrels, 1986). In a simple

isotope box model of the marine sulfur reservoir, variations in the isotopic

composition of marine sulfate are interpreted as being driven by relative

changes in these outputs, while typically assuming that the input of sulfur to the

ocean has remained constant through time. Recent work (Halevy et al., 2012) ,

however, has highlighted the need to consider changes in the flux and the

isotopic composition of sulfur to the ocean. Riverine sulfur is the major source of

sulfate to the ocean, supplying approximately 4.7 Tmol/y today (including 1.3

76   Tmol/y from anthropogenic sources (Meybeck, 2003)). Thus in order to fully

77   understand the secular changes in $\delta^{34}S$ of seawater, we need to better constrain

78   both the modern values for, and controls on, the isotopic composition of riverine

79   sulfate.

80   The modern riverine sulfur isotopic composition can also inform

81   estimates of chemical weathering fluxes, with important implications for the

82   carbon cycle. Sulfur isotopes in rivers can provide insight into how much

83   riverine S is sourced from dissolution of sedimentary sulfate minerals versus

84   oxidative weathering of pyrite (OWP)(Calmels et al., 2007). OWP produces

85   sulfuric acid, which is a source of acidity for chemical weathering and which,

86   when it interacts with carbonate minerals, can lead to a net release of CO_2, in

87   contrast to the sink of CO_2 associated with silicate weathering (e.g. Calmels et al.,

88   2007; Torres et al., 2016; 2015). Previous estimates of global OWP fluxes range

89   from 0.5 to 0.65 Tmol/y (Berner and Berner, 1996; Francois and Walker, 1992;

90   Lerman et al., 2007). However, recent studies that use sulfur isotopes (and

91   sulfate-oxygen isotopes) from individual catchments indicate that estimates of

92   global OWP flux are potentially much too low. The sum of OWP fluxes (0.15

93   Tmol/y) from just three river basins (Mackenzie (Calmels et al., 2007), Kaoping

94   (Das et al., 2012), and Jialing (Li et al., 2011)) can account for a third of previous

95   global OWP flux estimates, despite covering less than 2% of global land area (Das

96   et al., 2012). Underestimating global OWP by this magnitude may result in

97   substantial overestimates of the modern-day sink of CO_2 associated with

98   chemical weathering.

99

100

1.1 Previous estimates of $\delta^{34}S$ of river water

Previous estimates of the global sulfur isotopic composition of rivers

come from either measurements of river water from a single geographical region

(Ivanov et al., 1983) or back-of-the-envelope calculations based on simple

geochemical assumptions (Berner and Berner, 1996). The previous data-based

study that included the largest amount of river data was limited to the Eurasian

continent, and reported an average riverine $\delta^{34}S$ of 9.2‰ (Ivanov et al., 1983).

The rivers sampled represent only 7% of the total global riverine discharge and

have a total sulfate flux of 0.4 Tmol/y, accounting for only 9% of the total

riverine sulfate flux. The limited geographic extent of this estimate raises the

question of how representative the value of 9.2‰ is for the global riverine $\delta^{34}S$

input to the oceans, especially given that many of the rivers sampled are

weathering large evaporitic deposits of Cambrian/Ordovician age that are

exposed across the Siberian Platform (Huh et al., 1998b; Ivanov et al., 1983).

These deposits might bias the riverine $\delta^{34}S$ to high values, since evaporites have

$\delta^{34}S$ values reflecting the seawater $\delta^{34}S$ during the time of deposition, and range

from between 10 to 30‰ (e.g. Kampschulte and Strauss, 2004).

Geochemical calculations tend to form the basis of the most commonly

cited sulfur isotope compositions for modern riverine input estimates. Isotope

mass balance models of the sulfur cycle have typically employed a riverine $\delta^{34}S$

value of around 7-8‰ (e.g. Garrels and Lerman, 1984; Halevy et al., 2012; Kump

and Garrels, 1986; Kurtz et al., 2003). These values can be traced back to

assumptions about the relative contributions of sulfide and sulfate weathering to

the riverine sulfate budget. Specifically, it was assumed that the abundance of

sedimentary sulfate minerals is equal to the abundance of sedimentary sulfide

126   minerals and that gypsum weathers twice as fast as pyrite (Berner and Berner,

127   1996). These two assumptions imply that sulfate mineral weathering should

128   contribute twice as much sulfate to rivers as pyrite weathering. Thus, if a $\delta^{34}S$

129   value of 17‰ is assumed for sulfate in evaporite minerals and a $\delta^{34}S$ value of -

130   12‰ is assumed for pyrite, then a simple river isotope mass balance predicts an

131   average riverine $\delta^{34}S$ of between 7 to 8‰ (ignoring anthropogenic and other

132   minor sources of sulfate to rivers). It is important to note that because these

133   calculations assumed a fixed ratio of riverine sulfur from sulfide weathering to

134   sulfate weathering, this isotopic composition cannot then be used to calculate the

135   relative proportion of sulfide weathering. Nonetheless, this approach and its

136   origins are important and informative to the field.

137   Given the large uncertainties in these estimates of the relative fluxes in

138   the modern biogeochemical sulfur cycle, and the resulting implications for

139   weathering and the modern carbon cycle, the aims of this paper are to: (1) re-

140   evaluate the global modern sulfur isotopic composition of riverine sulfate, and

141   (2) estimate the modern flux of pyrite-derived sulfate supplied to the ocean from

142   rivers using two different and complementary methods: a weathering end-

143   member decomposition, and a simple sulfur isotope mass balance.

144

145   **2 Methods**

146   *2.1 Measurement of river water sulfate and $\delta^{34}S$*

147   River waters were sampled either opportunistically or as part of a

148   number of field campaigns between years 1993 – 2013. Details of all rivers

149   measured in this study for sulfur isotopes can be found in Supplementary Table

150   1. Previously published sulfur isotope data from main stems of rivers were

151   compiled from the literature, and can be found in Supplementary Table 2, along

152   with the new main stem data from this study. The locations of the main stems of

153   rivers included in this study can be seen in Figure 1.

154   The concentration of sulfate in river waters was determined by ion

155   chromatography with a Dionex ICS-2000, using an AS-19 column and 20 mM

156   KOH eluent at the Environmental Analysis Center at Caltech. River samples were

157   then dried down and re-dissolved in 0.01 M HCl. The sulfate was purified from its

158   matrix with an anion exchange column as described in Paris et al. (2014).

159   New measurements of sulfur isotopes in rivers were made by MC-ICP-MS

160   on a Neptune Plus at Caltech (Paris et al., 2013). Measurement by MC-ICP-MS

161   reduces sample size requirements by three orders of magnitude over traditional

162   gas source mass spectrometric methods, and thus only 20 nmol of sulfate were

163   needed for each sample. Typical rivers have micromolar concentrations of

164   sulfate, thus sample sizes were in the range of 100 uL to a few mL of river water

165   depending on concentration. An in-house sodium sulfate solution was used as a

166   bracketing standard on the MC-ICP-MS to correct for instrumental mass bias.

167   Consistency in chemistry and measurement was monitored with multiple full

168   replicates of a seawater standard (21.04 ± 0.17‰ V-CDT 2 s.d.; n = 20) and an

169   in-house consistency standard from a filtered river water sample collected from

170   the headwaters of the Arroyo Seco in Angeles National Forest, California near

171   Switzer Falls (4.11 ± 0.24‰ V-CDT 2 s.d.; n = 10).

172   Complete chemistry blanks were monitored along with every set of 10

173   samples, and contained an average of 0.1 nmol of sulfate. As the smallest samples

174   measured had 20 nmol of sulfate, the blank contamination contributes at most

175   0.5% of the total sulfate measured, and typically contributes closer to 0.1%, as

176   most samples were analyzed with at least 100 nmol of sulfate. The $\delta^{34}S$ of the

177   blank is typically close to zero, with a long-term average for all blanks of 2.4 ±

178   6.5‰ (2 s.d.; n = 16). The measured $\delta^{34}S$ of all river samples have been blank

179   corrected with the average of all blanks, and the uncertainty on both the amount

180   of blank and its isotopic ratio is propagated through to the final uncertainties on

181   the riverine $\delta^{34}S$ values.

182   Global average $\delta^{34}S$ values were calculated based on the data in

183   Supplementary Table 2. Sulfate fluxes were calculated for these main stem rivers

184   by multiplying sulfate concentration by discharge, and these fluxes were used to

185   calculate the global flux-weighted average and standard deviation of $\delta^{34}S$.

186

187   *2.2 End-member weathering calculation*

188   Previous studies have used coupled $\delta^{34}S$ and $\delta^{18}O$ in sulfate to estimate

189   OWP fluxes in individual river catchments (Calmels et al., 2007; e.g. Karim and

190   Veizer, 2000; Turchyn et al., 2013). These estimates do not rely on knowing the

191     $\delta^{34}S$ of the pyrite being weathered which can have a large range within an

192   individual basin (e.g. Calmels et al., 2007). This is a very powerful technique, but

193   measurement by gas source mass spectrometry requires larger sample sizes, and

194   has only been used on a few rivers, in contrast to the numerous $\delta^{34}S$

195   measurements on riverine sulfate that have been previously published. Thus, to

196   maximize the number of rivers included in our global database, we used riverine

197     $\delta^{34}S$ and major anion and cation concentrations in an end-member weathering

198   calculation following Gaillardet et al. (1999) to further constrain the global

199   budget of sulfide weathering.

200   Rivers that were either measured or compiled for $\delta^{34}S$ that also had Cl, Na,

201   Mg, Ca, and Sr concentration data (42 rivers total, representing 41% of the global

202   riverine discharge) were included in this end-member deconvolution. A

203   correction for atmospheric deposition from rainwater was made following

204   Gaillardet et al. (1997) based on the Cl concentration of the river. Each river was

205   assigned a critical value of Cl (ranging from 20 to 100 μM, Supplementary Table

206   2) based on the evapotranspiration factor of the river basin or nearby rivers

207   calculated from the GEMS-GLORI database (Meybeck and Ragu, 1995), and

208   typical values of Cl concentration in rainwater (14 μM, Moller, 1990). If the

209   concentration of Cl in the river was less than the critical value of Cl, then all of

210   the Cl in that river was attributed to rainwater and typical rainwater ratios of Na

211   to Cl (1.15) were used to determine the rainwater-derived fraction of Na for that

212   river. The remaining Na in the river was assumed to come from the weathering

213   of silicates, carbonates, and evaporites. If the concentration of Cl in the river was

214   greater than the critical value, it was assumed that the contribution of Cl from

215   rainwater was equal to the critical value for that river, with the remaining Cl

216   sourced from evaporites. Following the approach of Gaillardet et al. (1999), we

217   then used a series of linear equations to solve for the proportions of sodium in

218   the river that are attributed to evaporite, carbonate, and silicate weathering. The

219   linear equations for each river were solved 10,000 times using a random

220   sampling of weathering end-member values from a normal distribution of the

221   values and associated uncertainties listed in Table 1. The median and standard

222   deviation of these Monte Carlo simulations were used as the end-member

223   fraction and uncertainty for each river (see Supplementary Information).

224   We calculated the proportion of sulfate that could be attributed to each

225 end-member using the S/Na in the end-members (Table 1), and the S/Na

226 measured in the rivers following equation 1.

227

$$S_i = \frac{\left(\frac{S}{Na}\right)_i \alpha_i}{\left(\frac{S}{Na}\right)_{riv}}$$

228   Equation 1

229 where (S/Na) are molar ratios of sulfate to sodium, the subscript *i* refers to the

230 silicate, evaporite, carbonate, and rainwater end-members (Table 1), the

231 subscript *riv* refers to the riverine molar ratio, α is the fraction of sodium

232 attributed to each of the end-members (*i*) from the end-member weathering

233 calculation, and S_i is the fraction of sulfate in the river attributed to each of the

234 end-members (*i*). Any sulfate that cannot be attributed to one of the four end-

235 members, we call "excess sulfate". We used Monte Carlo simulations using the

236 end-member values and uncertainties from Table 1 as described above.

Table 1. End-member molar ratios (±2 s.d.)

Molar Ratio	Rain	Silicate	Carbonate	Evaporite
Ca/Na	0.023 ± 0.01	0.35 ± 0.25	60 ± 30	0.5 ± 0.5
Mg/Na	0.11 ± 0.01	0.25 ± 0.2	30 ± 15	0.1 ± 0.08
Sr/Na	0.0002 ± 0.0001	0.003 ± 0.001	0.04 ± 0.02	0.003 ± 0.002
Cl/Na	1.15 ± 0.1	-	-	1 ± 0.2
S/Na	0.06 ± 0.01	0.019 ± 0.005	0.06 ± 0.03	0.4 ± 0.2

237

238   Results of this calculation are sensitive to the end-member ratios selected,

239 especially for evaporites, which can vary widely. We use the Ca/Na, Mg/Na, and

240 Sr/Na end-member ratios for silicates and carbonates from Gaillardet et al.

241 (1999) and Negrel et al. (1993), and rainwater ratios from Berner and Berner

242 (1996) and Gaillardet et al. (1999). For evaporites, we calculate molar ratios

243 based on mineral abundances in evaporites given in Lerman et al. (2007),

244   assuming congruent weathering of evaporites. These evaporite based ratios are

245   consistent with the median ratio calculated from rivers that drain evaporites

246   (Meybeck, 1984; 1979), giving additional support for our choice of end-

247   members[1]. The S/Na value for carbonates is based on the S/Ca molar ratio of

248   0.001 in marine carbonates (Volkov and Rozanov, 1983) and the Ca/Na value of

249   carbonates of 60 (Negrel et al., 1993). Finally, the S/Na value of the silicate end-

250   member is calculated from global estimates of the abundance of S and Na_2O in

251   continental igneous and metamorphic rocks (Holser and Kaplan, 1966; Rudnick

252   and Gao, 2003). This estimate of S/Na in silicate rocks deliberately does not

253   include sedimentary sulfides (e.g. from shales). Consequently, any sulfate

254   derived from oxidative weathering of sedimentary pyrite would be incorporated

255   into the excess sulfate parameter described above.

256

257   **3 Results**

258   The river waters analyzed in this study yield a large range of $\delta^{34}S$ values,

259   between -13.4‰ and 21.7‰ (Figures 1 and 2), and represent more than 46% of

260   the global water discharge to the ocean (3.88 x 10^4 km^3/y (Peucker-Ehrenbrink,

261   2009)). This dataset includes smaller tributaries, as well as time series

262   measurements from individual major rivers (Fraser, Lena, Ob', Yenisei, Yukon,

263   Mackenzie, Kolyma, and Congo rivers). Within an individual river basin, there

264   can be a large range in the $\delta^{34}S$ of tributaries. For instance, $\delta^{34}S$ values from the

[1] The one exception to this statement is evaporite Mg/Na. The Mg/Na ratio based on mineral abundances is 0.03, while the Mg/Na ratio from rivers draining evaporites is 0.1. However, the final results are not sensitive to the choice of this parameter, with only a 0.02 Tmol/y difference in the estimate of the global flux of sulfate from evaporites, well within the uncertainty of the calculation (0.2 Tmol/y).

265   Congo River and its tributaries range from 3.7 to 12.5‰ (n = 7), those from the

266   Ganges River system range from -1 to 13.3‰ (n = 3), and those in the Amazon

267   River basin range from 4.5 to 13.4‰ (n= 19), though most of the Amazonian

268   tributaries have a narrow range of 4.5 to 7‰ (n=16), consistent with the

269   findings of Longinelli and Edmond (1983).

270   The $\delta^{34}S$ measured in river time series samples can also show a large

271   range, highlighting temporal heterogeneity in the isotopic composition of

272   riverine sulfate, that is likely driven by varying contributions from tributaries

273   that drain different lithologies (Figure 3). For instance the $\delta^{34}S$ of the Lena River

274   has a range of 7‰ between May and November, the $\delta^{34}S$ of the Mackenzie River

275   has a range of 4.5‰ between March and September, and the $\delta^{34}S$ of the Fraser

276   River has a range of 5‰ over the course of a year (Supplementary Table 1;

277   Figure 3). In contrast, time series data from the Congo, Kolyma, Ob', Yenisei, and

278   Yukon rivers have more constant (<2‰ variation) $\delta^{34}S$ over the course of

279   several months to a year (Supplementary Table 1).

280   The flux-weighted average of the rivers gives a $\delta^{34}S$ value of 4.4 ± 4.5‰

281   (1 s.d.). If the polluted rivers (([Na] – [Cl])/[Cl] < 0.1) are excluded[2] from this

282   estimate, the average $\delta^{34}S$ of riverine sulfate is 4.8 ± 4.9‰, and accounts for

283   more than 43% of the water discharge to the ocean. The similarity between these

284   two values suggests that the most polluted rivers do not meaningfully change the

---

[2] The only river with sufficient data to estimate a pre-anthropogenic, natural $\delta^{34}S$ and flux of sulfate is the Mississippi River. Killingsworth and Bao (2015) used an isotope mixing model to estimate a pre-anthropogenic $\delta^{34}S$ = -5‰, and a concentration of sulfate of 115 μM. This pre-anthropogenic estimate is *lower* than the measured $\delta^{34}S$ = -0.72‰ and sulfate concentration of 462 μM from this study (which is similar to the isotope and concentration measurements from 2009-2013 from (Killingsworth and Bao, 2015)).

285 estimate of the global riverine $\delta^{34}S$ value. We therefore take the value of 4.8‰

286 as our best estimate of the modern pre-anthropogenic $\delta^{34}S$ value of river water.

287 The flux-weighted distribution of the isotopic composition of riverine sulfate

288 (Figure 4) shows that half of the rivers have $\delta^{34}S$ values between 1.8 and 8.2‰

289 (interquartile range), including the rivers with the largest flux of sulfate (Amazon

290 and Yangtze rivers). Notable exceptions to this include the Mississippi and Lena

291 rivers, which contribute a large flux of sulfate to the oceans, but have low (-5‰)

292 and high $\delta^{34}S$ (19‰) values, respectively.

293   We can assess how representative our subset of rivers is of global riverine

294 discharge by comparing the flux-weighted Mg/Na and Ca/Na ratios and

295 strontium isotopes from our dataset with global estimates of these values from

296 previously published studies. Our flux weighted Mg/Na ratio of 0.66 and Ca/Na

297 ratio of 1.63 are within the range of previous global estimates of these values of

298 0.57 to 0.70 and 1.32 to 1.67, respectively (Meybeck and Ragu, 1995; Miller et al.,

299 2011). The same is true if we scale the river fluxes by the large scale drainage

300 regions (Graham et al., 1999; Peucker-Ehrenbrink and Miller, 2007) following

301 Miller et al. (2011). In this case, our subset of rivers yields a Mg/Na ratio of 0.68

302 and a Ca/Na ratio of 1.70, compared to previously published values of 0.55 to

303 0.71 and 1.27 to 1.74, respectively (Meybeck and Ragu, 1995; Miller et al., 2011).

304 Thus, our elemental ratios support the use of this subset of rivers for global

305 budget estimates. The flux weighted average $^{87}Sr/^{86}Sr$ ratio from our subset of

306 rivers with published ratios (40% of global water discharge) is 0.7115, slightly

307 higher than estimates of global riverine $^{87}Sr/^{86}Sr$ (0.7111 to 0.7114 (Peucker-

308 Ehrenbrink et al., 2010; Vance et al., 2009)). The slightly more radiogenic

309 $^{87}Sr/^{86}Sr$ value likely reflects an underrepresentation of younger, more

310   volcanically dominated river basins (e.g. smaller rivers on volcanic islands and

311   along active margins) in our subset of rivers. This might bias our estimate of

312   global riverine δ^{34}S to higher values, but the effect is likely small given that rivers

313   draining volcanic islands (e.g. Reunion, Iceland) have relatively low

314   concentrations of sulfate (34-70 μM) and have δ^{34}S values only slightly (1-3‰)

315   lower than our global average (Tables 1 and 2).

316

317   *3.1 Weathering end-member decomposition*

318   End-member decomposition allows us to tease apart the different sources

319   of sulfate to rivers. A plot of δ^{34}S of riverine sulfate versus the percentage of Na

320   derived from silicate weathering illustrates the importance of pyrite weathering

321   in influencing the sulfur isotopic composition of rivers (Figure 5). For rivers

322   with no Na derived from silicate weathering, the only other two sources of Na

323   are evaporite and carbonate minerals. As both of these lithologies reflect the

324   sulfur isotopic composition of seawater when they were formed, they should

325   both have high δ^{34}S values (~17‰, (Holser and Kaplan, 1966)). Similarly, for

326   rivers that derive 100% of their Na from silicate weathering (none from

327   evaporites or carbonates), the δ^{34}S of river water should be similar to the silicate

328   value of 4‰ (Holser and Kaplan, 1966). These two end-members determine the

329   red mixing lines in Figure 5. Most data plot below these mixing lines, implying a

330   ^{34}S-depleted source of sulfate to the rivers that does not also add Na. The

331   oxidative weathering of sedimentary pyrite could reasonably constitute such a

332   source.

333   We further quantify the sources of sulfate to rivers by using the end-

334   member values of S/Na from Table 1 and Equation 1 to convert fractional

335   contributions of Na from the different end-members into fractional contributions

336   of S from the different end-members. Based on our end-member decomposition,

337   evaporite weathering contributes 31 ± 6% (1.5 ± 0.2 Tmol/y) to the global

338   riverine sulfate budget. We find that the contribution of rainwater sulfate to

339   rivers in our database is minor, contributing about 1.6% (0.07 Tmol/y) to the

340   total riverine sulfate flux, consistent with independent estimates of the

341   contribution of cyclic sea salts (0.09 – 0.13 Tmol/y; (Berner and Berner, 1996;

342   Eriksson, 1963)) to riverine sulfate. The contribution of carbonate and silicate

343   weathering is also minor with only 0.01 and 0.09 Tmol/y derived from each of

344   those end-members, respectively.

345   The remaining sulfate in each river that cannot be readily attributed to

346   carbonate, silicate, and evaporite weathering, or to rainwater (sea-salt)

347   constitutes a parameter we call "excess sulfate". This "excess sulfate" is a

348   combination of the other major sources of sulfate to rivers: pollution, volcanic

349   atmospheric deposition, biogenic emissions, and the oxidative weathering of

350   sedimentary pyrite. This relative contribution of excess sulfate ranges from 0 to

351   more than 97% for all rivers, with the exception of the Narmada and Tapti rivers,

352   which have negative excess sulfate values. A negative excess sulfate value

353   implies that the sulfate in those rivers can be more than accounted for by

354   weathering of the three end-members and rainwater inputs, and thus could

355   indicate an unidentified sink for sulfate along the river (e.g. in the river flood

356   plain). For example, from sulfur isotope data it was suggested that removal of

357   riverine sulfate might occur via sulfate reduction and sulfide precipitation in

358   weakly developed soils in the Marsyandi River catchment in the Himalaya

359   (Turchyn et al., 2013). However, the extent to which this process occurs in other

360   river systems remains to be established (Torres et al., 2016). The excess sulfate

361   values thus represent minimum values, and for the remainder of this study we

362   will ignore the two rivers in our compilation that have a negative excess sulfate.

363   The flux weighted global percentage of excess sulfate is 65 ± 6% (3.1 ± 0.2

364   Tmol/y), which is dominated by pyrite weathering and pollution. The

365   contributions to riverine sulfate from volcanoes and biogenic emissions are both

366   relatively small (0.34 and 0.14 Tmol/y, respectively (Berner and Berner, 1996)).

367   Using an estimate of the pollutive sulfate in rivers of 1.3 Tmol/y (Meybeck,

368   2003), we estimate that the global contribution of oxidative weathering of pyrite

369   to riverine sulfate is 1.3 Tmol/y, or about 28% of the total sulfate flux from all

370   sources to the ocean (4.7 Tmol/y), and 46% of the flux of sulfate from

371   weathering (i.e. 2.8 Tmol/y, excluding sulfate from pollution, volcanoes, biogenic

372   emissions, and cyclic sea salts).

373

374   4 **Discussion**

375   *4.1 Controls on riverine sulfate $\delta^{34}S$*

376   The highest $\delta^{34}S$ values measured (14.4 to 21.7‰) come from the Lena

377   and Yenisei rivers which drain the Siberian Platform—a region of large evaporite

378   and carbonate platforms deposited from late Proterozoic through Paleozoic time

379   (Huh et al., 1998b). Since these rocks are abundant in sulfate phases derived

380   from seawater, they are characterized by relatively high $\delta^{34}S$ values. The sulfate

381   minerals weather readily, resulting in both high concentrations of sulfate and

382   high $\delta^{34}S$ values for these rivers. The lowest $\delta^{34}S$ values (-8.5 to -13.4‰) come

383   from tributaries of the Santa Clara River (e.g. Sespe) in Southern California,

384   which weather sandstones, siltstones, and organic-rich shales of the Monterey

385   Formation and equivalent units. Sedimentary evaporites are absent from the

386   underlying strata, and thus sulfate in these rivers is likely dominated by the

387   oxidation of pyrite and organic sulfur molecules, which, due to the biological

388   isotope fractionations associated with sulfate reduction in organic-rich

389   sediments during their diagenesis and lithification, results in lower overall $\delta^{34}S$

390   values. The lowest $\delta^{34}S$ values measured in major rivers come from the Orinoco

391   (-5.1‰) and the Kolyma (-4.2 to -5.6‰) rivers, which also drain catchments

392   rich in sedimentary rocks, including black shales (Edmond et al., 1996; Huh et al.,

393   1998a). These examples are consistent with the notion that local lithology plays

394   a key role in setting the sulfur isotopic composition of rivers, and the important

395   role of black shale weathering in the sulfur budget.

396   Plots of the $\delta^{34}S$ versus inverse concentration of sulfate and versus the

397   riverine Na/SO_4 ratio (Figure 2) show a triangular pattern, indicative of at least

398   three end-members contributing to sulfate in rivers. The most sulfate-rich rivers

399   span a wide range of $\delta^{34}S$ values (-13 to 21‰), whereas the rivers with the

400   lowest sulfate concentrations cluster tightly between ~5-10 ‰. Rivers plotting

401   in the high concentration-high $\delta^{34}S$ region, such as the Lena River, are likely

402   dominated by sulfate minerals weathered from evaporites. Gypsum ($CaSO_4$)

403   dissolves easily, and rivers draining evaporitic rocks usually have high

404   concentrations of total dissolved solids, including sulfate. These rivers have

405   Na/S values ranging between 1.7 and 5, consistent with an evaporite end-

406   member.

407   Rivers plotting in the high concentration-low $\delta^{34}S$ region could have

408   sulfate sources dominated by the oxidative weathering of pyrite, which has low

409   $\delta^{34}S$ values, or by pollution, which is often cited in the literature as having low or

410   negative $\delta^{34}S$ signatures (e.g. Ivanov et al., 1983). We screened for polluted

411   rivers using ancillary anion and cation data (Fiege et al., 2009; Miller et al., 2011;

412   Peterson et al., 2016; Voss et al., 2014). If the value of $([Na] - [Cl])/[Cl]$ is less

413   than 0.1, then the river is considered polluted. The main sources of Cl to rivers

414   are sea salt aerosols, evaporites, and pollution. As both sea salt aerosols and

415   evaporites deliver Na and Cl in roughly equal proportions, an excess of Cl relative

416   to Na may be indicative of a polluted river. The following rivers have high Cl

417   relative to Na: Connecticut, Danube, Indus, Doubs, Lena, Mississippi, Neman,

418   Rhine, Seine, and St. Lawrence. These rivers are also located near large human

419   populations or near industrial centers. The one exception to this is the Lena

420   River, which is influenced by Cl-rich brines (Gaillardet et al., 1999). As shown in

421   Figure 2, the polluted rivers tend to have high sulfate concentrations (>100 μM,

422   with the exception of the Doubs whose main sulfate sources are atmospheric

423   (Calmels et al., 2014)). However, there is a large range of $\delta^{34}S$ for these rivers;

424   thus they do not simply populate the bottom left of the graph, as would be

425   expected if pollution always had a low $\delta^{34}S$ signature. Indeed, measurements of

426    $\delta^{34}S$ on oil, gas, coal and sulphide ores range from -25 to +30‰ (Newman et al.,

427   1991), and $\delta^{34}S$ of fertilizers, another anthropogenic sulfate source, can range

428   from -6.5 to 20.7‰ (Szynkiewicz et al., 2011; Vitoria et al., 2004). Since pollution

429   cannot be the sole reason for the high sulfate concentration and low $\delta^{34}S$, it

430   follows that the oxidation of pyrite is a major source of sulfate to these rivers.

431   This is consistent with the abundance of shales and pyrites in the catchment

432   areas of the rivers (e.g. the Kolyma (Huh et al., 1998a), Orinoco (Edmond et al.,

433   1996), Buller (Robinson and Bottrell, 1997), Kaoping (Das et al., 2012), Skeena

434   (Spence and Telmer, 2005), and Stikine rivers (Calmels et al., 2007)).

435   Rivers and tributaries with low concentrations of sulfate (e.g. Amazon,

436   Congo, and Niger rivers) tend to have $\delta^{34}S$ values of 5 - 10‰ (Figure 2). The low

437   sulfate concentrations likely reflect the lack of any significant weathering of

438   evaporites or pyrite-rich shales in these drainage basins. Their low

439   concentration of sulfate could also be attributed in part to the large flow of water

440   and the dilution of solutes, as the concentration of total dissolved solids for these

441   rivers is low at 35-59 mg/L (Meybeck and Ragu, 1995). However, the small range

442   of $\delta^{34}S$ values indicates a similar source of sulfate to the rivers, leaving us to

443   conclude that silicate weathering of igneous rock and atmospheric deposition of

444   sulfate (sea salts) are the major sources of sulfate to these rivers and tributaries,

445   consistent with previous studies (Negrel et al., 1993; Gaillardet et al., 1997).

446   Rivers with a high ratio of Na/S also plot within this narrower range of $\delta^{34}S$,

447   consistent with a silicate or atmospheric source.

448   The wide range in $\delta^{34}S$ from tributaries from an individual river basin

449   (e.g. Congo , Ganges, Mackenzie) highlights the spatial heterogeneity of sulfur

450   sources to rivers, that is most likely controlled by heterogeneity of the bedrock

451   geology—and commensurate differences in the isotopic composition of the

452   sulfur-bearing phases—in their catchments. The differences in the temporal

453   variability of $\delta^{34}S$ between individual river basins indicate that some rivers (e.g.

454   Lena, Mackenzie, and Fraser) have weathering conditions that are more

455   heterogeneous than other river basins with more constant $\delta^{34}S$, and that the

456   varied lithologies in these river catchments contribute differently to the

457   dissolved load at distinct times throughout the year. For instance, in the case of

458   the Fraser River, the δ^{34}S of sulfate over the course of a year shows a strong

459   correlation (r^2 = 0.88) with the dissolved ^{87}Sr/^{86}Sr ratio in these waters (Voss et

460   al., 2014). Dissolved ^{87}Sr/^{86}Sr values decrease along the flow path of the Fraser

461   River reflecting the underlying geology, as the river flows from

462   Precambrian/Paleozoic sedimentary rocks of the Rocky Mountains, through the

463   young, magmatic and metamorphic rocks of the Coast Range (Cameron and

464   Hattori, 1997). The time series data indicate a greater relative contribution of the

465   Coast Range to the dissolved ion budget during the winter. The sulfur isotope

466   compositions imply that during the winter months, more sulfate is derived from

467   the oxidative weathering of ^{34}S-poor sulfide-bearing phases in the Coast Range,

468   whereas during the summer a greater proportion of the sulfate derives from

469   sulfate minerals within Paleozoic strata.

470   The importance of pyrite weathering in setting the δ^{34}S value of rivers

471   globally can be seen in Figure 6. This figure shows the relationship between the

472   measured δ^{34}S versus the δ^{34}S values predicted from a sulfur isotope mass

473   balance in each river based on the weathering end-member decomposition. This

474   sulfur isotope mass balance uses the proportion of sulfate derived from the

475   weathering and rain water end-members and assumes end-member δ^{34}S values

476   of 17‰ for evaporite and carbonate weathering, 4‰ for silicate weathering,

477   and 20‰ for rainwater (Herut et al., 1995; Holser and Kaplan, 1966). The 1:1

478   line in Figure 6 indicates rivers whose measured δ^{34}S values can be entirely

479   accounted for by sulfur input from sources besides pyrite weathering and

480   pollution. Most rivers plot to the left of this line indicating that the measured

481   values of δ^{34}S are lower than predicted. Furthermore, the rivers that plot farthest

482   from the line have large excess sulfate proportions (calculated from the end-

483   member decomposition), implying that the sulfur isotopic composition of this

484   excess sulfate has a low $\delta^{34}S$ value, consistent with a pyrite source[3].

485

486   *4.2 Global dissolved sulfur isotope mass balance for rivers*

487   The riverine $\delta^{34}S$ values reported here (4.4±4.5‰ and 4.8 ± 4.9‰

488   excluding the most polluted rivers) are lower than the previous compilation

489   value from Eurasian rivers of 9‰ (Ivanov et al., 1983) and the values of 7 to 8‰

490   typically used in models of the global sulfur cycle (Halevy et al., 2012; e.g. Kump

491   and Garrels, 1986; Kurtz et al., 2003). At face value these lower values of the $\delta^{34}S$

492   of rivers implies that a greater fraction of riverine sulfate derives from reduced

493   sources (e.g. pyrite) than previously estimated. This finding is in line with recent

494   studies illustrating the high relative contribution of oxidative weathering of

495   pyrite to riverine sulfate based on detailed studies of individual river basins (e.g.

496   Mackenzie (Calmels et al., 2007), Kaoping (Das et al., 2012) , Marysandi (Turchyn

497   et al., 2013), Amazon (Torres et al., 2016) and Ganges-Brahmaputra (Galy and

498   France-Lanord, 1999)), and we can now expand those conclusions to the global

499   budget.

500   Using a simple terrestrial weathering isotope mass balance akin to that

501   used in Kump and Garrels (1986), we can calculate the fraction of pyrite

502   weathering contributing to riverine sulfate:

503

504        $f_{owp} = -(\delta_{evap} - \delta_{riv})/(\delta_{py} - \delta_{evap})$ Equation 2

505

---

[3] Note that the most polluted rivers (see text) have been excluded from these calculations and figures.

506   where f_{owp} is the fraction of pyrite-derived sulfate, δ_{evap} is the $\delta^{34}S$ of evaporite

507   (17‰ (Holser and Kaplan, 1966)), δ_{riv} is the $\delta^{34}S$ of riverine sulfate (4.8‰,

508   above), and δ_{py} is the $\delta^{34}S$ of pyrite from sedimentary rocks (-12‰ (Holser and

509   Kaplan, 1966)). This gives a f_{owp} in rivers of 0.42, substantially higher than the

510   estimate of f_{owp} of 0.28 if the riverine $\delta^{34}S$ value is taken to be 9‰ (Ivanov,

511   1983).

512   These estimates are very sensitive to the assumption of the end-member

513    $\delta^{34}S$ values of the oxidized (sulfate salts) and reduced (sulfide and disulfide)

514   sedimentary reservoirs, which are difficult to constrain from a global

515   perspective. Estimates of the global $\delta^{34}S$ values of oxidized S in sediments range

516   from 12.1‰ to 19‰, and of reduced sediments from -7.4‰ to -16‰ (Holser et

517   al., 1988 and references therein). These different combinations of δ_{evap} and δ_{py}

518   give a range of f_{owp} between 0.35 to 0.42 (compared to f_{owp} = 0.16 to 0.29 if the

519   river $\delta^{34}S$ value is taken to be 9‰), with a median f_{owp} of 0.41. Despite the large

520   uncertainties in the correct end-member isotope values, the estimate of f_{owp} =

521   0.41 is broadly consistent with the independently derived fluxes from the

522   weathering end-member decomposition that indicate that pyrite weathering

523   contributes up to 46% of the sulfate flux in rivers due to weathering. The

524   weathering end-member decomposition is based solely on major ion

525   concentrations and not isotope values, and so is independent of the isotope mass

526   balance calculation in Equation 2.

527

528   *4.3 Implications for the modern sulfur cycle and marine isotope mass balance*

529   Our flux estimate of riverine sulfate from evaporite weathering (1.5

530   Tmol/y) that we derived from weathering end-member decomposition is larger

531   than the assumed value of 1 Tmol/y of sulfate weathering by Berner and

532   Raiswell (1983) and Garrels and Lerman (1981), which is widely used in box

533   models of the sulfur cycle and is smaller than the value estimated more recently

534   by Lerman et al. (2007) (1.98 Tmol/y). Our estimate of the sulfide weathering

535   flux from the weathering end-member decomposition (1.3 Tmol/y) is about

536   twice as large as the commonly cited estimates of the global OWP flux (0.5-0.64

537   Tmol/y (Berner and Berner, 1996; Lerman et al., 2007)), and is consistent with

538   our estimate from an isotope mass balance discussed in the previous section that

539   is based on the revised global average riverine $\delta^{34}S$ value of 4.8‰. Thus the

540   isotope and river chemistry data independently imply a larger contribution of

541   oxidative weathering of pyrite to the riverine sulfate flux than previously

542   estimated[4].

543   It can be informative to investigate the derivation of previous estimates of

544   the sulfate flux from OWP in order to understand why they were significantly

545   lower than our new value. Previous estimates of global OWP from Berner and

546   Berner (1996) and Lerman et al. (2007) both relied on assumptions of the

547   relative abundance of pyrite in sedimentary rocks, though they do this

548   differently. The 0.5 Tmol/y estimate (Berner and Berner, 1996) assumed that the

549   riverine ratio of calcium from weathering of sedimentary rocks to pyrite-derived

550   sulfate must be the same as the ratio of calcium to pyrite sulfur in common

---

[4] In order to close the riverine sulfate budget, previous estimates attributed any remaining sulfate that did not derive from pyrite or evaporite weathering to pollution (e.g. Berner and Berner, 1996), rather than using an independent estimate of sulfate pollution (Meybeck, 2003) as we have done here.

551   sedimentary rocks (which was taken to be 8.5 and 0.3 weight % of calcium and

552   pyrite-S, giving a molar pyrite-S/Ca ratio of 0.04 (Garrels and Lerman, 1984)).

553   The molar ratios of excess sulfate/Ca from our end-member decomposition are

554   more typically around 0.1 and can be as high as 0.6 for catchments with

555   abundant shales (e.g. Kolyma (Huh et al., 1998a), Orinoco (Edmond et al., 1996),

556   and Kaoping (Das et al., 2012)). Thus the assumed ratio of calcium to pyrite

557   sulfur in common sedimentary rocks might not fully account for the presence of

558   pyrite-rich shales. The OWP flux estimate of 0.64 Tmol/y (Lerman et al., 2007)

559   assumes that 24% of sedimentary sulfur is in the reduced form of pyrite. This

560   percentage is significantly lower than previous estimates, which are closer to

561   50% (e.g. Holser et al., 1988 and references therein). Thus both of these prior

562   estimates potentially underestimated the global abundance of pyrite S in

563   sedimentary rocks by a factor of two, which could help to explain the

564   underestimation of global OWP fluxes.

565   Our revised estimate of the OWP flux is similar to the estimate of global

566   pyrite burial in ocean sediments calculated from the estimates of global organic

567   carbon burial and the C/S value in modern sediments (1.22 Tmol/y; (Berner,

568   1982)). It is also similar to the upper range of estimates of pyrite burial (36% of

569   the total natural, pre-anthropogenic flux) based on marine isotope mass balance

570   and constraints from marine $\delta^{33}S$ (Tostevin et al., 2014). Our upward revision of

571   global pyrite weathering brings the oceanic input and output of reduced sulfur,

572   which previously differed by a factor of 2, into close agreement.

573   The uncertainties on these modern fluxes from the weathering end-

574   member decomposition of river concentration data alone are still too large (0.2

575   Tmol/y) to assess whether the modern sulfur cycle is in steady state with regard

576   to the relative amounts of oxidized and reduced sulfur that are weathered and

577   buried. However, if we assume steady-state, our new riverine $\delta^{34}S$ value can be

578   used in a marine isotope mass balance that solves for the fraction of the sulfate

579   removed from the ocean through pyrite burial (f_{pyr}):

580

581                    $$f_{pyr} = (\delta_{riv} - \delta_{sw})/(\Delta^{34}S_{pyrite-seawater}) \qquad\qquad \text{Equation 3}$$

582

583   where δ_{sw} is the $\delta^{34}S$ of seawater (21‰; (Paris et al., 2013)) and $\Delta^{34}S_{pyrite-seawater}$

584   is the isotope fractionation between seawater sulfate and sedimentary pyrite in

585   the modern ocean (δ_{py} - δ_{sw}). A plot of the solutions to Equation 3 for our new

586   value for δ_{riv} (4.8‰) and the previous value for δ_{riv} (9‰) is shown in Figure 7

587   for a range of $\Delta^{34}S_{pyrite-seawater}$. Our lower value of δ_{riv} = 4.8‰ implies that there is

588   a greater fraction of pyrite burial than previously predicted based on a δ_{riv} = 9‰.

589   Using this model to determine a specific value for the modern fraction of pyrite

590   burial is not currently possible because the global average value of $\Delta^{34}S_{pyrite-}$

591    $_{seawater}$ is difficult to constrain given the large range of $\delta^{34}S$ values measured in

592   modern pyrites.

593   If, however, we assume that the fraction of pyrite burial (f_{pyr}) is equivalent

594   to the fraction of pyrite weathered (f_{owp}) as calculated either by the weathering

595   end-member decomposition from major ion chemistry (0.46) or riverine isotope

596   mass balance (0.41), then our data suggest that $\Delta^{34}S_{pyrite-seawater}$ should be -35‰

597   or -39‰, respectively. These estimates are roughly consistent with canonical

598   assumptions of, $\Delta^{34}S_{pyrite-seawater}$ = -35‰ (e.g. Garrels and Lerman, 1981), but are

599   much more positive than flux weighted estimates of this value based on pyrite

600   measurements from modern continental shelf, slope and rise sediments

601   ($\Delta^{34}S_{pyrite-seawater}$ = -48‰(Yu Lein et al., 1983)). Modelling studies that use

602   constraints from $\delta^{33}S$ also predict a greater difference between the $\delta^{34}S$ values of

603   seawater and bulk pyrite buried ($\Delta^{34}S_{pyrite-seawater}$ = -56 ± 5‰) (Tostevin et al.,

604   2014). These larger offsets in the isotopic composition of seawater and buried

605   pyrite would imply that the fraction of pyrite buried is 0.29 and 0.34 for $\Delta^{34}S_{pyrite-}$

606    $_{seawater}$ = -56 and $\Delta^{34}S_{pyrite-seawater}$ = -48, respectively (Figure 7), significantly less

607   than our two independent estimates of the fraction of pyrite weathered. If

608   correct, these estimates indicate that the biogeochemical sulfur cycle may not be

609   balanced, and that more pyrite is being weathered than is being buried in

610   modern marine sediments. This conclusion would be consistent with recent ice

611   core evidence that shows a decrease in atmospheric O_2 over the past 800,000

612   years (Stolper et al., 2016). The magnitude of the imbalance between weathering

613   and burial fluxes of reduced carbon and sulfur that is required to explain the long

614   term oxygen trend in ice cores is ~2% (Stolper et al., 2016); this number is well

615   within uncertainties of the weathering flux estimates (~0.2 Tmol/y). However,

616   given the large range of estimates of $\Delta^{34}S_{pyrite-seawater}$ more work constraining

617   global $\Delta^{34}S_{pyrite-seawater}$ from modern sediments would help to resolve this issue.

618   Our increased estimate of global OWP means that the previously

619   published OWP rates from three river basins (Mackenzie (Calmels et al., 2007),

620   Kaoping (Das et al., 2012), and Jialing (Li et al., 2011)) only account for ~12%

621   (rather than a third) of the total global OWP flux estimate. Nonetheless, the fact

622   that these rivers drain less than 2% of global surface area highlights the

623   heterogeneity of pyrite weathering; simply put, some river basins will contribute

624   disproportionately to the global pyrite weathering budget, based on their

625   tectonic and geological characteristics. The spatial heterogeneity of pyrite

626   weathering thus has important implications for the long-term variations in the

627   δ^{34}S of riverine input: changes in paleogeography, paleohydrology, eustasy, and

628   the formation and uplift of sedimentary basins will change both the amounts and

629   types of rock exposed to weathering, which in turn will likely change the value of

630   riverine δ^{34}S input to the oceans through time.

631   Finally, the increased estimate of the OWP flux has implications for the

632   modern carbon cycle and carbon-weathering feedbacks. As pyrite oxidation

633   coupled to carbonate weathering can provide a source of CO_2 to the atmosphere

634   (e.g. Calmels et al., 2007; Das et al., 2012; Lerman et al., 2007; Torres et al., 2016;

635   2015), the greater flux of pyrite-derived sulfate indicates a more significant role

636   for this process in the modern biogeochemical sulfur and carbon cycles. Modern

637   weathering and carbon budgets should be reassessed on a global scale to account

638   for an increased global contribution from OWP.

639

640   **5 Conclusion**

641   We determined the modern δ^{34}S value of riverine sulfate to be 4.4 ±

642   4.5‰, based on measurements of rivers that account for more than 46% of

643   global freshwater discharge. Removing highly polluted rivers from the estimate

644   gives a similar δ^{34}S value of riverine sulfate of 4.8 ± 4.9‰. These δ^{34}S values are

645   lower than previous estimates of the isotopic composition of riverine sulfate, and

646   imply a greater contribution of pyrite weathering to riverine sulfate than has

647   previously been assumed. An end-member decomposition of weathering

648   sources to these rivers indicates that the relative contributions of evaporite

649   (sulfate) and pyrite (sulfide) weathering to riverine sulfate budgets are ~1.5 and

650   1.3 Tmol S/y, respectively. This estimate of pyrite weathering is twice as high as

651   previous estimates, and is consistent with isotope mass balance constraints on

652   the $\delta^{34}S$ of river water that imply that ~40% of non-anthropogenic riverine

653   sulfate derives from weathered pyrite. Since pyrite oxidation can act as a source

654   of CO_2 to the atmosphere, this new estimate should reduce the global carbon sink

655   attributed to chemical weathering. Basin lithology exerts a strong control on the

656    $\delta^{34}S$ values of riverine sulfate, questioning the validity of assuming constant $\delta^{34}S$

657   of riverine input to the ocean over geological time. Stratigraphic trends observed

658   in sulfur isotopes in ancient sedimentary rocks might therefore reflect secular

659   changes in the isotopic composition of the riverine inputs, rather than changes in

660   the relative burial of marine pyrite versus sulfate salt evaporites.

661

662   **6 Acknowledgements**

668
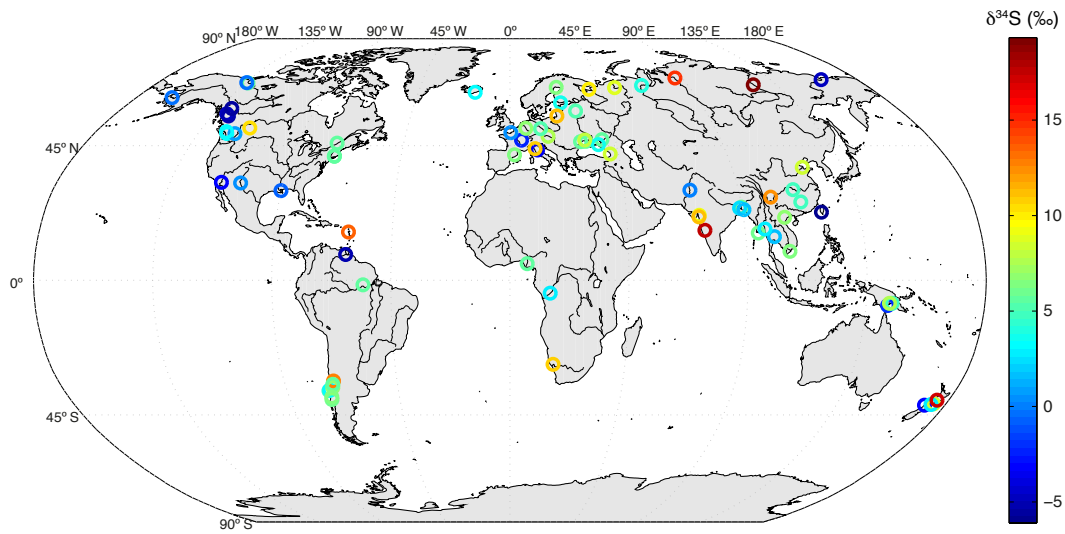
Figures

Figure 1. Global map of measured and compiled main stem river $\delta^{34}S$ values ($‰$, V-CDT) that contribute to the global flux-weighted average of 4.4$‰$. The variation seen between these major rivers relates to differences in catchment geology.

675
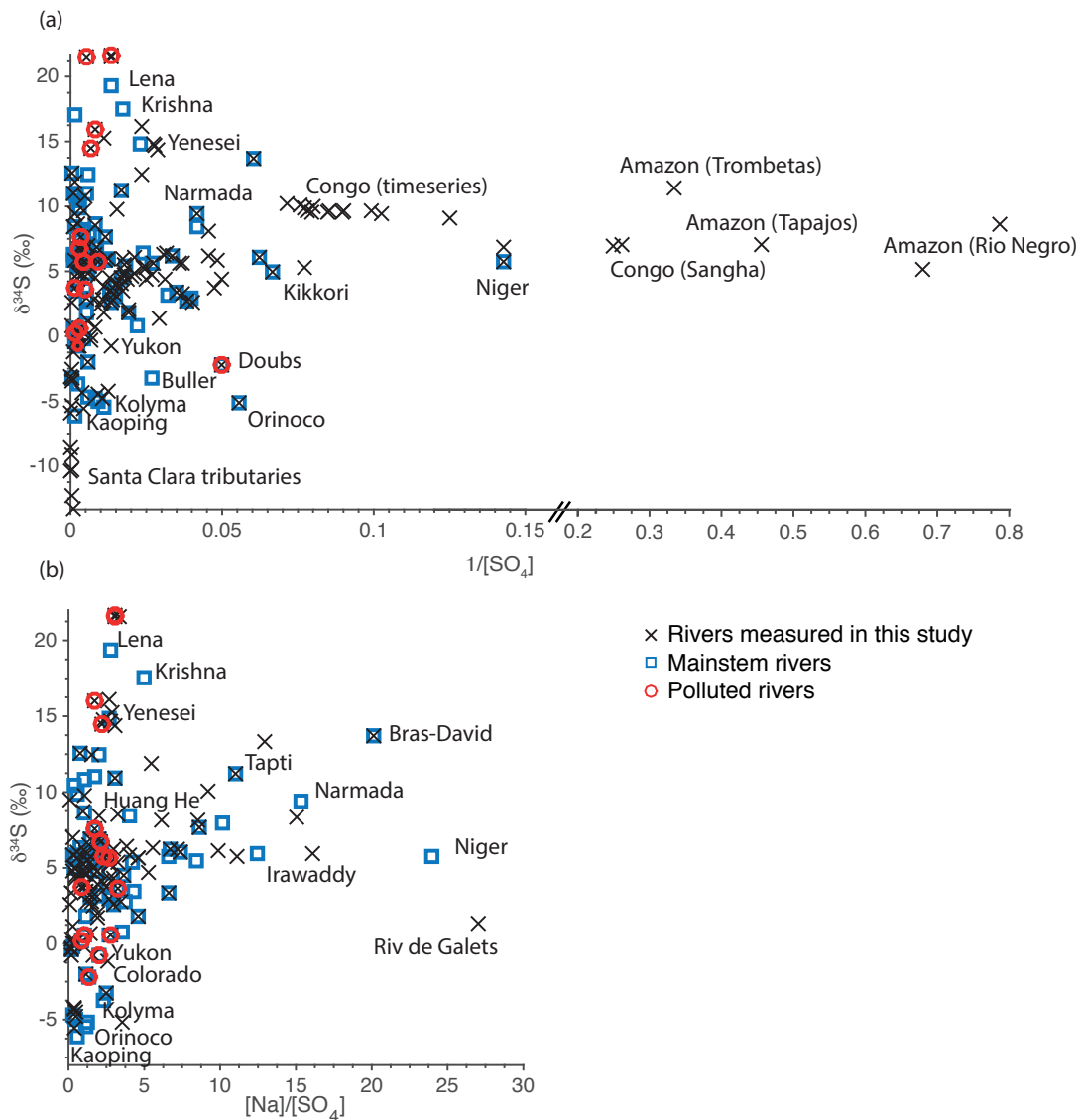
Figure 2. (a) $\delta^{34}S$ values (‰, V-CDT) of all rivers measured versus the inverse

concentration (μM^{-1}) of sulfate (black x). Rivers designated as main stem rivers

(compiled or measured) are shown as blue squares. Rivers identified as being

polluted (section 4.1) are circled in red. Note the change in scale on the X-axis

after the break. (**b**) Same as above but plotted against the Na/SO_4 molar value of

the riverine dissolved load.

682
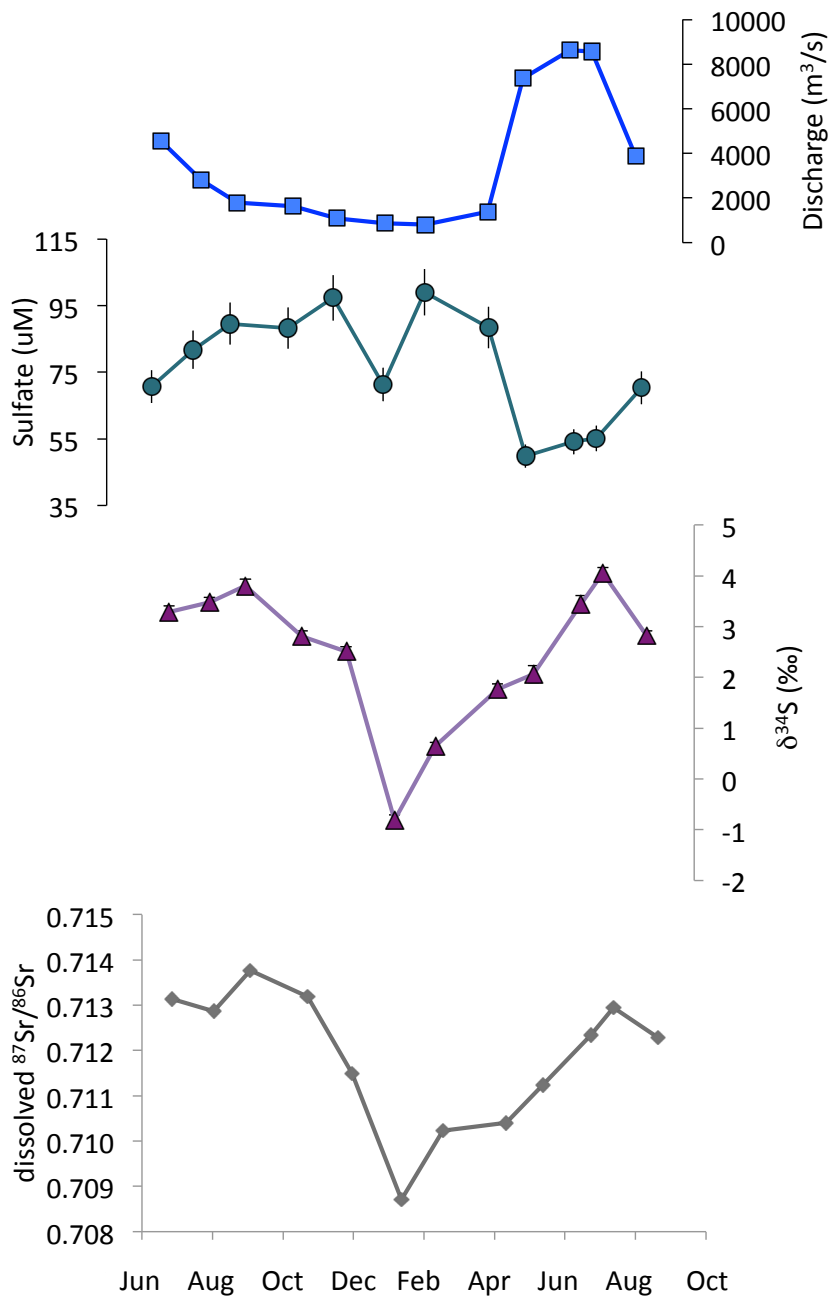
683
684 **Figure 3.** Time series data from Fraser River samples collected between June

685 2010 and August 2011. (a) Freshwater discharge (m³/s), (b) sulfate

686 concentration (µM); (c) δ³⁴S values (‰, V-CDT), (d) ⁸⁷Sr/⁸⁶Sr from (Voss et al.,

687 2014).

688
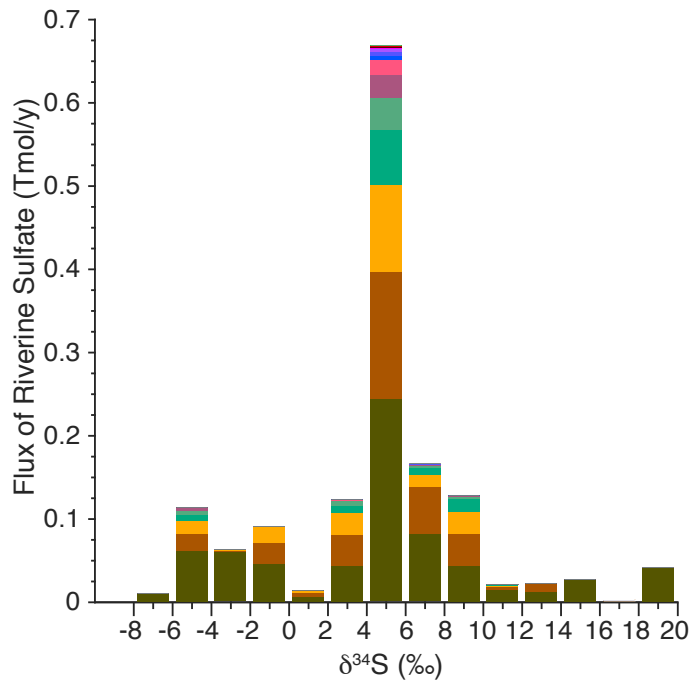
Figure 4. Stacked bar graph showing the $\delta^{34}S$ values (‰, VCDT) and the flux of

sulfate from individual main stem rivers that contribute to the global flux-

weighted average $\delta^{34}S$ value of 4.4‰. Each color represents a different river.

692
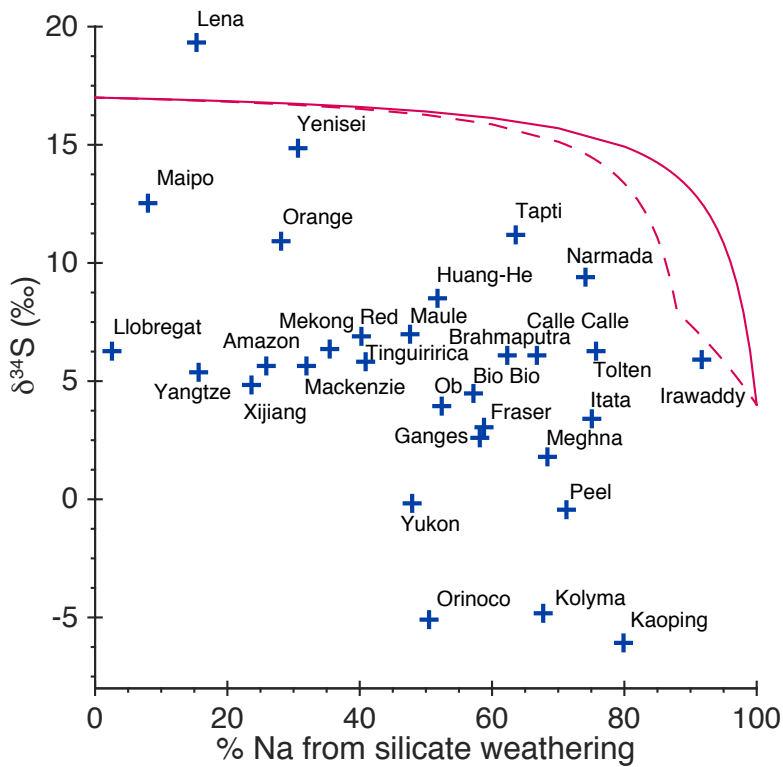
Figure 5. Riverine $\delta^{34}S$ values (‰, V-CDT) of main stem rivers as a function of
the percent of Na attributed to silicate weathering from the end-member
decomposition. The red solid line is the predicted $\delta^{34}S$ based on a riverine
isotope mass balance, using the S/Na end-member ratios from Table 1, and
assuming that the $\delta^{34}S$ value of silicate rocks is 4‰, that the $\delta^{34}S$ value of
evaporites is 17‰, and that there is no contribution of Na from carbonates. The
red dashed line is the predicted $\delta^{34}S$ based on a riverine isotope mass balance,
using the S/Na end-member ratios from Table 1, and assuming that the $\delta^{34}S$
value of silicate rocks is 4‰, that the $\delta^{34}S$ value of evaporites and carbonates is
17‰, and that carbonates contribute 12% of the Na (maximum contribution
found for all rivers in this study), with the remainder coming from silicates and
evaporites.

705
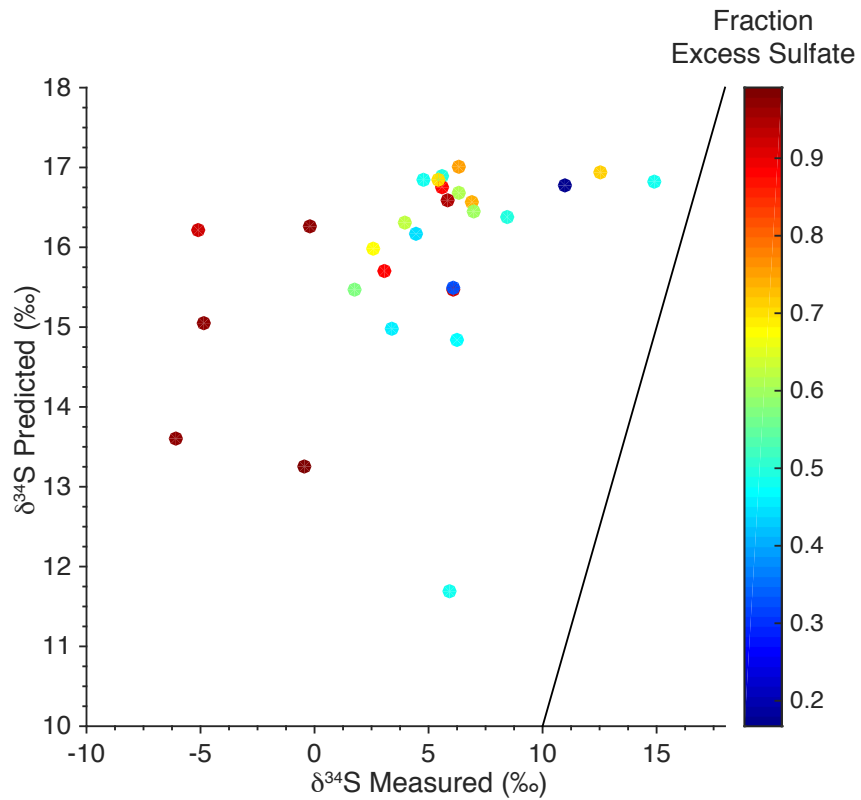
706
707 **Figure 6.** Plot of predicted $\delta^{34}S$ (based on assumptions of end-members from

708 mixing model, see section 4.1) versus measured $\delta^{34}S$ values (‰, V-CDT). The

709 black line is the 1:1 line. The colors indicate the fraction of excess sulfate. Rivers

710 plotting to the left of the line have more negative $\delta^{34}S$ values than predicted, and

711 thus are likely influenced by oxidative weathering of pyrite.

712
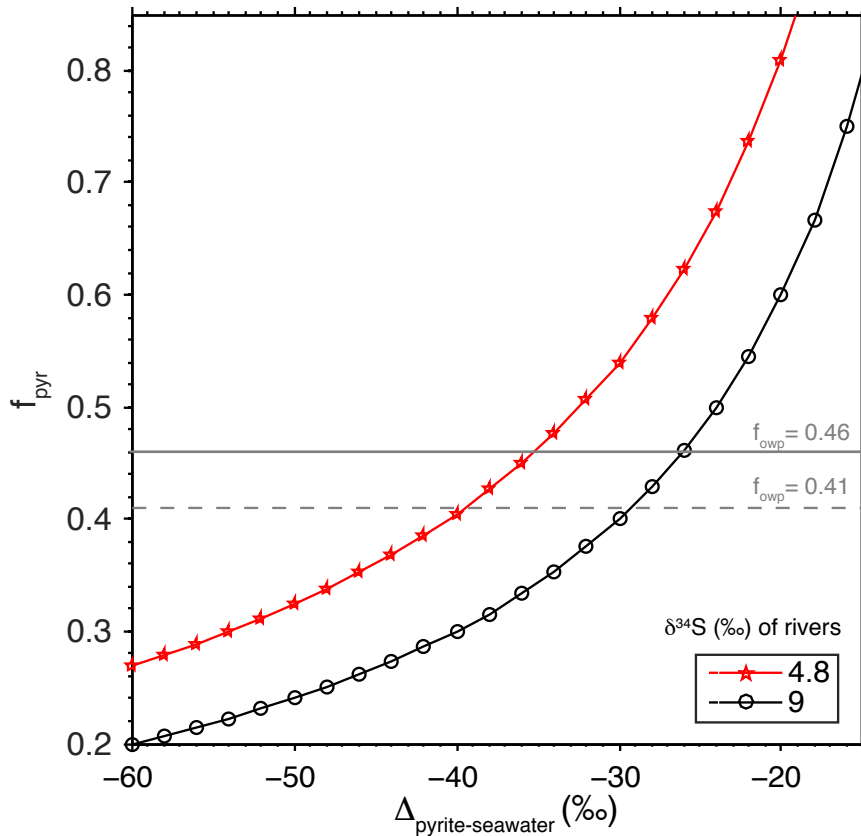
Figure 7. Sensitivity of the proportion of sulfur buried marine basins as pyrite

(f_{pyr}) as a function of the fractionation ($\Delta_{pyrite-seawater}$, ‰) between reduced and

oxidized sulfur for a given riverine sulfate $\delta^{34}S$ value, and assuming steady state

isotope mass balance in the ocean. The red line with stars represents our

estimate of the modern riverine $\delta^{34}S$ value from this study (4.8‰). Previous

compilations of the riverine $\delta^{34}S$ value were higher (~9‰, black circles; (Ivanov

et al., 1983)). Estimates of the relative contribution of weathering of pyrite (f_{owp})

to modern riverine sulfate from our two independent approaches are shown for

reference (f_{owp} = 0.46 (solid line, based on our weathering end-member

decomposition from major ion chemistry of the rivers) and f_{owp} = 0.41 (dashed

line, based on riverine isotope mass balance)).

724
725

References

Berner, E.K., Berner, R.A., 1996. Global environment: water, air, and geochemical cycles. Prentice Hall, New York.

Berner, R.A., 1982. Burial of organic carbon and pyrite sulfur in the modern ocean; its geochemical and environmental significance. Am J Sci 282, 451–473. doi:10.2475/ajs.282.4.451

Berner, R.A., Raiswell, R., 1983. Burial of Organic-Carbon and Pyrite Sulfur in Sediments Over Phanerozoic Time - a New Theory. Geochimica et Cosmochimica Acta 47, 855–862.

Calmels, D., Gaillardet, J., Brenot, A., France-Lanord, C., 2007. Sustained sulfide oxidation by physical erosion processes in the Mackenzie River basin: Climatic perspectives. Geology 35, 1003. doi:10.1130/G24132A.1

Calmels, D., Gaillardet, J., François, L., 2014. Sensitivity of carbonate weathering to soil CO2 production by biological activity along a temperate climate transect. Chemical Geology 390, 74–86. doi:10.1016/j.chemgeo.2014.10.010

Cameron, E.M., Hattori, K., 1997. Strontium and neodynium isotope ratios in the Fraser River, British Columbia: a riverine transect across the Cordilleran orogen. Chemical Geology 137, 243–253. doi:10.1016/S0009-2541(96)00168-4

Das, A., Chung, C.-H., You, C.-F., 2012. Disproportionately high rates of sulfide oxidation from mountainous river basins of Taiwan orogeny: Sulfur isotope evidence. Geophys. Res. Lett. 39, n/a–n/a. doi:10.1029/2012GL051549

Edmond, J.M., Palmer, M.R., Measures, C.I., Brown, E.T., Huh, Y., 1996. Fluvial geochemistry of the eastern slope of the northeastern Andes and its foredeep in the drainage of the Orinoco in Colombia and Venezuela. Geochimica et Cosmochimica Acta 60, 2949–2974. doi:10.1016/0016-7037(96)00142-1

Eriksson, E., 1963. The yearly circulation of sulfur in nature. Journal of Geophysical Research 68, 4001–4008.

Fiege, K., Miller, C.A., Robinson, L.F., Figueroa, R., Peucker-Ehrenbrink, B., 2009. Chemical Geology. Chemical Geology 268, 337–343. doi:10.1016/j.chemgeo.2009.09.013

Francois, L.M., Walker, J.C.G., 1992. Modelling the Phanerozoic carbon cycle and climate; constraints from the 87 Sr/ 86 Sr isotopic ratio of seawater. Am J Sci 292, 81–135. doi:10.2475/ajs.292.2.81

Gaillardet, J., Dupré, B., Allegre, C.J., Negrel, P., 1997. Chemical and physical denudation in the Amazon River basin. Chemical Geology 142, 141–173.

Gaillardet, J., Dupré, B., Louvat, P., Allegre, C.J., 1999. Global silicate weathering and CO2 consumption rates deduced from the chemistry of large rivers. Chemical Geology 159, 3–30.

Galy, A., France-Lanord, C., 1999. Weathering processes in the Ganges–Brahmaputra basin and the riverine alkalinity budget. Chemical Geology.

Garrels, R.M., Lerman, A., 1984. Coupling of the sedimentary sulfur and carbon cycles; an improved model. Am J Sci 284, 989–1007. doi:10.2475/ajs.284.9.989

Garrels, R.M., Lerman, A., 1981. Phanerozoic Cycles of Sedimentary Carbon and Sulfur. Proc. Natl. Acad. Sci. U.S.A. 78, 4652–4656.

Graham, S.T., Famiglietti, J.S., Maidment, D.R., 1999. Five-minute, 1/2°, and 1° data sets of continental watersheds and river networks for use in regional

775 and global hydrologic and climate system modeling studies. Water Resources
776 Research 35, 583–587. doi:10.1029/1998WR900068

777 Habicht, K.S., Canfield, D.E., 2001. Isotope fractionation by sulfate-reducing
778 natural populations and the isotopic composition of sulfide in marine
779 sediments. Geology 29, 555–558. doi:10.1130/0091-
780 7613(2001)029<0555:IFBSRN>2.0.CO;2

781 Halevy, I., Peters, S.E., Fischer, W.W., 2012. Sulfate Burial Constraints on the
782 Phanerozoic Sulfur Cycle. Science 337, 331–334.
783 doi:10.1126/science.1220224

784 Herut, B., Spiro, B., Starinsky, A., Katz, A., 1995. Sources of sulfur in rainwater as
785 indicated by isotopic δ34S data and chemical composition, Israel.
786 Atmospheric Environment 29, 851–857. doi:10.1016/1352-2310(94)00307-
787 7

788 Holser, W.T., Kaplan, I.R., 1966. Isotope geochemistry of sedimentary sulfates.
789 Chemical Geology 1, 93–135. doi:10.1016/0009-2541(66)90011-8

790 Holser, W.T., Schidlowski, M., Mackenzie, F.T., Maynard, J.B., 1988. Geochemical
791 cycles of carbon and sulfur, in: Gregor, C.B., Garrels, R.M., Mackenzie, F.T.,
792 Maynard, J.B. (Eds.), Chemical Cycles in the Evolution of the Earth. Wiley,
793 New York, pp. 105–173.

794 Huh, Y., Panteleyev, G., Babich, D., Zaitsev, A., Edmond, J.M., 1998a. The fluvial
795 geochemistry of the rivers of Eastern Siberia: II. Tributaries of the Lena,
796 Omoloy, Yana, Indigirka, Kolyma, and Anadyr draining the
797 collisional/accretionary zone of the Verkhoyansk and Cherskiy ranges.
798 Geochimica et Cosmochimica Acta 62, 2053–2075. doi:10.1016/S0016-
799 7037(98)00127-6

800 Huh, Y., Tsoi, M.Y., Zaitsev, A., Edmond, J.M., 1998b. The fluvial geochemistry of
801 the rivers of eastern Siberia: I. Tributaries of the Lena River draining the
802 sedimentary platform of the Siberian Craton. Geochimica et Cosmochimica
803 Acta 62, 1657–1676.

804 Ivanov, M.V., 1983. Major Fluxes of the Global Biogeochemical Cycle of Sulphur
805 , in: Ivanov, M.V., Freney, J.R. (Eds.), The Global Biogeochemical Sulphur Cycle.
806 New York, pp. 449–463.

807 Ivanov, M.V., Grinenko, V.A., Rabinovich, A.P., 1983. The Sulphur Cycle in
808 Continental Reservoirs, in: Ivanov, M.V., Freney, J.R. (Eds.), The Global
809 Biogeochemical Sulphur Cycle, Sulphur Flux From Continents to Oceans. New
810 York, pp. 331–356.

811 Kampschulte, A., Strauss, H., 2004. The sulfur isotopic evolution of Phanerozoic
812 seawater based on the analysis of structurally substituted sulfate in
813 carbonates. Chemical Geology 204, 255–286.
814 doi:10.1016/j.chemgeo.2003.11.013

815 Karim, A., Veizer, J., 2000. Weathering processes in the Indus River Basin:
816 implications from riverine carbon, sulfur, oxygen, and strontium isotopes.
817 Chemical Geology 170, 153–177.

818 Killingsworth, B.A., Bao, H., 2015. Significant Human Impact on the Flux and δ
819 34S of Sulfate from the Largest River in North America. Environ. Sci. Technol.
820 49, 4851–4860. doi:10.1021/es504498s

821 Kump, L.R., Garrels, R.M., 1986. Modeling Atmospheric O-2 in the Global
822 Sedimentary Redox Cycle. Am J Sci 286, 337–360.

823 Kurtz, A.C., Kump, L.R., Arthur, M.A., Zachos, J.C., Paytan, A., 2003. Early Cenozoic

824   decoupling of the global carbon and sulfur cycles. Paleoceanography 18, n/a–
825   n/a. doi:10.1029/2003PA000908

826 Lerman, A., Wu, L., Mackenzie, F.T., 2007. CO2 and H2SO4 consumption in
827   weathering and material transport to the ocean, and their role in the global
828   carbon balance. Marine Chemistry 106, 326–350.
829   doi:10.1016/j.marchem.2006.04.004

830 Li, X.D., Liu, C.Q., Liu, X.L., Bao, L.R., 2011. Identification of dissolved sulfate
831   sources and the role of sulfuric acid in carbonate weathering using dual-
832   isotopic data from the Jialing River, Southwest China. Journal of Asian Earth
833   Sciences. doi:10.1016/j.jseaes.2011.06.002

834 Li, Y.H., 1972. Geochemical mass balance among lithosphere, hydrosphere and
835   atmosphere. Am J Sci.

836 Longinelli, A., Edmond, J.M., 1983. Isotope geochemistry of the Amazon basin: a
837   reconnaissance. Journal of Geophysical Research 88, 3703–3717.

838 Meybeck, M., 2003. Global Occurrence of Major Elements in Rivers, in: Drever, J.I.
839   (Ed.), Treatise on Geochemistry. Elsevier, pp. 207–223.

840 Meybeck, M., 1984. Les fleuves et le cycle géochimique des éléments.

841 Meybeck, M., 1979. Concentrations des eaux fluviales en éléments majeurs et
842   apports en solution aux océans. Revue de Geologie Dynamiqe et de
843   Geographie Physique 21, 215–246.

844 Meybeck, M., Ragu, A., 1995. GEMS/Water contribution to the global register of
845   river inputs (GLORI), Provisional Final Report. UNEP/WHO/UNESCO,
846   Geneva, Geneva. doi:10.1029/2010GC003259/full

847 Miller, C.A., Peucker-Ehrenbrink, B., Walker, B.D., Marcantonio, F., 2011. Re-
848   assessing the surface cycling of molybdenum and rhenium. Geochimica et
849   Cosmochimica Acta 75, 7146–7179. doi:10.1016/j.gca.2011.09.005

850 Moller, D., 1990. The Na/Cl ratio in rainwater and the seasalt chloride cycle.
851   Tellus, Series B 42 B, 254–262. doi:10.1034/j.1600-0889.1990.t01-1-00004.x

852 Negrel, P., Allegre, C.J., Dupré, B., Lewin, E., 1993. Erosion Sources Determined by
853   Inversion of Major and Trace-Element Ratios and Strontium Isotopic-Ratios
854   in River Water - the Congo Basin Case. Earth and Planetary Science Letters
855   120, 59–76.

856 Newman, L., Krouse, H.R., Grinenko, V.A., 1991. Sulphur Isotope Variations in the
857   Atmosphere, in: Krouse, H.R., Grinenko, V.A. (Eds.), Stable Isotopes: Natural
858   and Anthropogenic Sulphur in the Environment. John Wiley & Sons, pp. 133–
859   176.

860 Paris, G., Adkins, J.F., Sessions, A.L., Webb, S.M., Fischer, W.W., 2014. Neoarchean
861   carbonate-associated sulfate records positive 33S anomalies. Science 346,
862   739–741. doi:10.1126/science.1258211

863 Paris, G., Sessions, A.L., Subhas, A.V., Adkins, J.F., 2013. MC-ICP-MS measurement
864   of δ 34 S and∆ 33 S in small amounts of dissolved sulfate. Chemical Geology
865   345, 50–61. doi:10.1016/j.chemgeo.2013.02.022

866 Peterson, B., Holmes, R.M., McClelland, J.W., Tank, S., Raymond, P.A., 2016. Arctic
867   Great Rivers Observatory 1 Biogeochemistry Data (2009 - 2011).
868   doi:10.18739/A2ZQ03

869 Peucker-Ehrenbrink, B., 2009. Land2Sea database of river drainage basin sizes,
870   annual water discharges, and suspended sediment fluxes. Geochem.-
871   Geophys.-Geosyst. 10, n/a–n/a. doi:10.1029/2008GC002356

872 Peucker-Ehrenbrink, B., Miller, M.W., 2007. Quantitative bedrock geology of the

873 continents and large-scale drainage regions. Geochem.-Geophys.-Geosyst. 8,
874   doi:10.1029/2006GC001544

875 Peucker-Ehrenbrink, B., Miller, M.W., Arsouze, T., Jeandel, C., 2010. Continental
876   bedrock and riverine fluxes of strontium and neodymium isotopes to the
877   oceans. Geochem.-Geophys.-Geosyst. 11, doi:10.1029/2009GC002869

878 Robinson, B.W., Bottrell, S.H., 1997. Discrimination of sulfur sources in pristine
879   and polluted New Zealand river catchments using stable isotopes. Applied
880   Geochemistry 12, 305–319. doi:10.1016/S0883-2927(96)00070-4

881 Rudnick, R.L., Gao, S., 2003. Composition of the continental crust. Treatise on
882   Geochemistry 3, 1–64. doi:10.1016/B0-08-043751-6/03016-4

883 Sim, M.S., Ono, S., Donovan, K., Templer, S.P., Bosak, T., 2011. Effect of electron
884   donors on the fractionation of sulfur isotopes by a marine Desulfovibrio sp.
885   Geochimica et Cosmochimica Acta 75, 4244–4259.
886   doi:10.1016/j.gca.2011.05.021

887 Spence, J., Telmer, K., 2005. The role of sulfur in chemical weathering and
888   atmospheric CO2 fluxes: Evidence from major ions, δ13CDIC, and δ34SSO4 in
889   rivers of the Canadian Cordillera. Geochimica et Cosmochimica Acta 69,
890   5441–5458. doi:10.1016/j.gca.2005.07.011

891 Stolper, D.A., Bender, M.L., Dreyfus, G.B., Yan, Y., Higgins, J.A., 2016. A Pleistocene
892   ice core record of atmospheric O2 concentrations. Science 353, 1427–1430.
893   doi:10.1126/science.aaf5445

894 Szynkiewicz, A., Szynkiewicz, A., Witcher, J.C., Witcher, J.C., Modelska, M.,
895   Modelska, M., Borrok, D.M., Borrok, D.M., Pratt, L.M., 2011. Anthropogenic
896   sulfate loads in the Rio Grande, New Mexico (USA). Chemical Geology 283,
897   194–209. doi:10.1016/j.chemgeo.2011.01.017

898 Torres, M.A., West, A.J., Clark, K.E., Paris, G., Bouchez, J., Ponton, C., Feakins, S.J.,
899   Galy, V., Adkins, J.F., 2016. The acid and alkalinity budgets of weathering in
900   the Andes–Amazon system: Insights into the erosional control of global
901   biogeochemical cycles. Earth and Planetary Science Letters 450, 381–391.
902   doi:10.1016/j.epsl.2016.06.012

903 Torres, M.A., West, A.J., Li, G., 2015. Sulphide oxidation and carbonate dissolution
904   as a source of CO. Nature 507, 346–349. doi:10.1038/nature13030

905 Tostevin, R., Turchyn, A.V., Farquhar, J., Johnston, D.T., Eldridge, D.L., Bishop,
906   J.K.B., McIlvin, M., 2014. Multiple sulfur isotope constraints on the modern
907   sulfur cycle. Earth and Planetary Science Letters 396, 14–21.
908   doi:10.1016/j.epsl.2014.03.057

909 Turchyn, A.V., Tipper, E.T., Galy, A., Lo, J.-K., Bickle, M.J., 2013. Isotope evidence
910   for secondary sulfide precipitation along the Marsyandi River, Nepal,
911   Himalayas. Earth and Planetary Science Letters 374, 36–46.
912   doi:10.1016/j.epsl.2013.04.033

913 Vance, D., Teagle, D.A., Foster, G.L., 2009. Variable Quaternary chemical
914   weathering fluxes and imbalances in marine geochemical budgets. Nature
915   458, 493.

916 Vitoria, L., Otero, N., Soler, A., Canals, À., 2004. Fertilizer Characterization:
917   Isotopic Data (N, S, O, C, and Sr). Environ. Sci. Technol. 38, 3254–3262.
918   doi:10.1021/es0348187

919 Volkov, I.I., Rozanov, A.G., 1983. The Sulfur Cycle in Oceans, in: The Global
920   Biogeochemical Sulphur Cycle, Reservoirs and Fluxes. John Wiley & Sons,
921   New York, pp. 357–423.

922 Voss, B.M., Peucker-Ehrenbrink, B., Eglinton, T.I., Fiske, G., Wang, Z.A., Hoering,
923   K.A., Montluçon, D.B., LeCroy, C., Pal, S., Marsh, S., Gillies, S.L., Janmaat, A.,
924   Bennett, M., Downey, B., Fanslau, J., Fraser, H., Macklam-Harron, G., Martinec,
925   M., Wiebe, B., 2014. Tracing river chemistry in space and time: Dissolved
926   inorganic constituents of the Fraser River, Canada. Geochimica et
927   Cosmochimica Acta 124, 283–308. doi:10.1016/j.gca.2013.09.006
928 Yu Lein, A., Grinenko, V.A., Migdisov, A.A., 1983. The Sulphur Cycle in Oceans, in:
929   The Global Biogeochemical Sulphur Cycle, The Mass-Isotopic Balance of
930   Sulphur in Oceanic Sediments. John Wiley & Sons, New York, pp. 423–448.
931